Journal of Materials Chemistry B

ROYAL SOCIETY OF CHEMISTRY

PAPER

View Article Online
View Journal | View Issue

Cite this: J. Mater. Chem. B, 2025, 13, 5655

Calcium phosphate bone cements with α-ketoglutarate polyester microspheres promote osteoporotic bone defect repair†

Zhengyang Kang, ‡[abc] Hui Yang,‡[ab] Xinzhi Liang,[ab] Bin Wu,[c] Dequan Wang,[c] TingLiang Xiong,[c] Luhui Zhang*[ab] and Denghui Xie*[ab]

Excessive oxidative stress and inflammation are prevalent in osteoporotic bone defects, significantly impairing the efficacy of bone regeneration in such defects. Calcium phosphate bone cements (CPC) are a commonly employed material for repairing bone defects. However, the slow rate of osteogenic mineralization and biodegradation presents a significant challenge in meeting the requirements of osteoporotic bone treatment. In this study, α-ketoglutarate (α-KG) polyester microspheres were synthesized from α-KG. By introducing different mass ratios of α-KG polyester microspheres, we constructed CPC with α-KG polyester microspheres (CPC/α-KG) that exhibited an improved microenvironment, enhanced osteogenic differentiation, and increased biomineralization. The incorporation of α-KG polyester microspheres was instrumental in enhancing the physicochemical attributes, biodegradability, biocompatibility, osteogenic differentiation potential, and biomineralization of α-KG. Mechanistically, the CPC/α-KG improves the osteogenic microenvironment by inhibiting the inflammatory response and reducing oxidative stress through the *PI3K/AKT* signaling pathway. Notably, the addition of 10 wt% α-KG polyester microspheres resulted in the optimal osteogenic capacity for CPC/α-KG. In conclusion, the modified α-KG composites show potential as effective candidates for bone defect repair and regeneration.

Received 19th February 2025,
Accepted 4th April 2025

DOI: 10.1039/d5tb00380f

rsc.li/materials-b

1. Introduction

As the aging population grows, the prevalence of osteoporosis has increased markedly.[1] Osteoporotic fractures are typified by poor bone mass, slow repair, weak internal fixation stability, and a high failure rate, and are frequently accompanied by varying degrees of bone defects,[1,2] which represents a significant challenge in clinical practice. The primary issues associated with osteoporotic bone defects can be attributed to two fundamental factors: cellular senescence and deficient osteogenic environment.[3,4] Therefore, improving the cellular state and osteogenic environment may be an effective strategy to improve the outcome of osteoporotic bone defects.

In cases of osteoporotic bone defects, the primary method of repair is the utilization of exogenous implants. Autologous grafts are frequently regarded as the gold standard for bone grafting due to their excellent biocompatibility and non-immunogenicity.[5] Nevertheless, the number of autologous bone donors is small and a secondary surgical procedure is often required.[6] Furthermore, autologous bone grafts are associated with an increased risk of complications, including inflammation, infection, bleeding, and pain, which significantly restrict their clinical application.[7] Allograft represents the second most common method of bone grafting and is a more widely available source of allograft bone than autograft.[8] However, its lack of cellular components and thus reduced osteoinductive properties and potential immune reactions are not favorable for its clinical promotion.[8,9] Therefore, the development of bone graft materials with high osteogenic efficacy is not only clinically important but also represents an urgent scientific challenge.

Artificial bone repair materials include two main types: organic polymeric materials (*e.g.* polylactic acid, gelatin, and chitosan, *etc.*) and inorganic polymeric materials (hydroxyapatite, calcium phosphate bioactive materials, bioactive ceramic materials, *etc.*).[10,11] Among these materials, calcium phosphate cements (CPC) can degrade and be absorbed *in vivo*, subsequently

[a] *Department of Joint Surgery and Sports Medicine, Center for Orthopedic Surgery, the Third Affiliated Hospital, Southern Medical University, Guangzhou, 510630, P. R. China. E-mail: smuspine@163.com*
[b] *Guangdong Provincial Key Laboratory of Bone and Joint Degeneration Diseases, Guangzhou, 510630, P. R. China*
[c] *Department of Orthopedics, The Second People's Hospital of Panyu Guangzhou, Guangzhou, 511400, P. R. China*

† Electronic supplementary information (ESI) available. See DOI: https://doi.org/10.1039/d5tb00380f

‡ ZK and HY contributed equally to this work.

being replaced by new tissues.[12] CPC exhibit many advantages, including good biocompatibility, ease of shaping, and osteoconductivity.[13] They were clinically applied in the area of bone tissue replacement and repair and are regarded as promising bone repair materials for clinical application. However, CPC are inorganic salt materials, and thus osteogenic induction and osteomineralisation are slow, biodegradation is slow, and the scope of clinical application is still limited.[13,14] Therefore, further improving the performance of CPC is of great importance to broaden their clinical applications.

Recent research has provided evidence that α-KG can promote osteogenic differentiation and exert anti-inflammatory and antioxidant effects.[15,16] α-KG directly addresses the core problems of osteoporotic defects, poor cellular status, and inadequate osteogenic microenvironment. In a previous study, Yousaf *et al.*[17] synthesized poly(triol-α-ketoglutarate, POA) through the condensation of α-KG with either 1,2,6-hexanediol or 1,2,4-butanediol. The resulting POA shows remarkable mechanical properties, including high tensile strength, good flexibility and outstanding impact resistance, which can be attributed to the formation of a well – ordered and compact molecular structure through the ester bond – mediated connections between molecular chains. In terms of chemical properties, POA exhibits excellent chemical stability and corrosion resistance, mainly because of the relatively high bond energy of the ester bonds within its molecular structure. Mangal *et al.* combined α-KG polymeric nanoparticles with methotrexate for the treatment of murine rheumatoid arthritis and modulation of T-cell response.[18] Interestingly, polymer microspheres can obviously improve the degradation performances of CPC.[19] Therefore, we believe that incorporating α-KG into polymer microspheres is a promising strategy.

In this study, CPC/α-KG-based active materials were constructed to improve the pathological microenvironment of osteoporosis. 10 wt% α-KG polyester microspheres were introduced into the structure of CPC, bringing a twofold advantage: the bioactivity of the bone cement was increased. Specifically, the release of α-KG through the hydrolysis of α-KG polyester added to the CPC significantly enhanced its bioactivity. Simultaneously, the antioxidant, anti-inflammatory, and osteogenic properties of CPC were also enhanced. The capacity of the material to improve the pathological microenvironment of osteoporosis was validated at both the cellular and animal levels. Moreover, this addition also accelerated the degradation of CPC, which in turn facilitated *in situ* osteogenesis. The findings of this research will provide novel insights and a theoretical foundation for the utilization of CPC materials, and offer new material options for the treatment of clinical osteoporotic bone defects.

2. Materials and methods

2.1. Raw materials

The following materials were obtained from Macklin Biochemical Co., Ltd, with specified purity and particle size: α-KG (98% purity, 80–100 mesh), 1,10-decanediol (98% purity, liquid form), α-tricalcium triphosphate (α-TCP) (95% bioceramic grade, 1–10 μm), DCPA (Dicalcium Phosphate Anhydrous) (99% purity, 60–80 mesh), ethyl orthosilicate (99% purity, liquid), triethyl phosphate (99% industrial grade, liquid), and calcium nitrate (98% purity, 50–100 mesh), sodium dihydrogen phosphate (NaH_2PO_4)(≥99% purity, 60–80 mesh), disodium hydrogen phosphate (Na_2HPO_4)(≥99% purity, 80–100 mesh).

Prior to use, all powdered materials (α-TCP, DCPA, calcium nitrate, NaH_2PO_4, and Na_2HPO_4) were dried at 80 °C for 24 h and sieved through appropriate mesh screens (80 mesh) to ensure uniformity. Liquid reagents (*e.g.*, 1,10-decanediol, ethyl orthosilicate) were used as received. The phosphate buffer solution (PBS) used in this study was a 0.1 M aqueous solution prepared by mixing sodium dihydrogen phosphate (NaH_2PO_4) and disodium hydrogen phosphate (Na_2HPO_4) at pH 7.4.

2.2. Synthesis of CPC/α-KG

In a round-bottom flask, an equimolar ratio of 1 : 1 of α-KG and 1,10-decanediol was prepared. The mixture was stirred at 130 °C under nitrogen for 48 hours. The resulting polymer was precipitated in a methanol solution, and the unreacted monomer was removed using multiple precipitations, at least three time. Subsequently, the residual methanol was evaporated. The polymer was subjected to vacuum drying at 25 °C for 48 hours, yielding α-KG polyester. Subsequently, a mixed solution comprising water, ethanol, organic solvents, and surfactants was prepared, and ethyl orthosilicate, catalyst, triethyl phosphate, and calcium nitrate were added sequentially and stirred thoroughly to obtain the α-KG polyester gel solution. The α-KG polyester solution was subjected to centrifugation and washing, causing the formation of a wet gel precipitate. This precipitate was subsequently placed in an oven for drying, thereby obtaining α-KG polyester microsphere powder.

The alpha-tricalcium triphosphate (α-TCP) powder and the sodium dihydrogen phosphate (NaH_2PO_4) powder were combined in accordance with a molar ratio of 1.5 : 1. The resulting mixture was stirred thoroughly to ensure homogeneous distribution. This procedure was employed to prepare the CPC powder, which was then stored for future use. Subsequently, the α-KG polyester microsphere powder was homogeneously blended with CPC powder at mass ratios of 0 : 10 (0 wt% α-KG), 1 : 9 (10 wt% α-KG), 2 : 8 (20 wt% α-KG), and 3 : 7 (30 wt% α-KG), using a turbula powder mixer (SYH-10, Changzhou Yibu Drying Equipment Co., China) at 50 rpm for 30 minutes. The blended composite powder was mixed with a curing liquid (0.25 mol L^{-1} NaH_2PO_4 solution) at a powder-to-liquid ratio (P/L) of 2 : 5 (g mL^{-1}). The resulting paste was immediately injected into cylindrical molds (3 mm diameter × 2 mm thickness) and cured at 25 °C with 50% humidity for 24 hours to fabricate standardized CPC/α-KG samples.

2.3. Characterization of CPC/α-KG

2.3.1. XRD. The phase composition of the samples was analyzed by XRD (D/MAX-RB, Rigaku Inc.). After the samples were pulverized, they were continuously scanned in the range of

10° to 70° over a rate of 4° min^{-1} to obtain a complete diffraction pattern.

2.3.2. SEM. The morphology of samples was observed using a SEM (Hitachi S-4800, JEOL, Japan). To image the morphology of the composites, the samples were fixed on a sample stage, sprayed with gold, and photographed.

2.3.3. Mechanical strength. To evaluate the mechanical properties of CPC/α-KG including its compressive modulus and tensile modulus, the following experimental procedures were conducted. Cylindrical specimens with a diameter of 6 mm and height of 12 mm were fabricated in accordance with ASTM D695 standards. The end surfaces of the specimens were polished using sandpaper to ensure parallelism and flatness. Uniaxial compression testing was performed using an electronic universal testing machine (Instron 5967, USA) at a crosshead displacement rate of 1 mm min^{-1}.

For tensile testing, dumbbell-shaped specimens with a gauge length of 12 mm, width of 4 mm, and thickness of 2 mm were prepared. The same testing machine was employed for uniaxial tensile testing under identical displacement control (1 mm min^{-1}). The stress–strain relationship was recorded during the tensile process, and the tensile modulus was calculated from the linear elastic region of the curve. All mechanical tests were conducted under controlled environmental conditions at 25 °C.

2.3.4. Anti-washout ability. To evaluate the erosion resistance and stability of CPC/α-KG under physiological fluid flow conditions, a dynamic fluid scouring test was conducted using an *in vitro* circulatory system. The experimental setup incorporated a peristaltic pump (flow rate range: 10–100 mL min^{-1}) to simulate dynamic fluid environments, with phosphate-buffered saline (PBS, pH 7.4) serving as the simulated body fluid (SBF). Bone cement specimens, prepared according to ASTM F451 standards, were fixed in a flow chamber to ensure exposure to a stable flow field. The experiments were performed under controlled conditions at 37 °C using a thermostatic water bath. Three flow rates (10, 50, and 100 mL min^{-1}) were selected to mimic low-shear (tissue fluid), medium-shear (venous flow), and high-shear (arterial flow) hydrodynamic environments. Specimens were subjected to scouring durations of 24, 48, and 72 hours for each flow rate group. Mass changes of the samples were measured periodically using an electronic analytical balance to quantify erosion resistance and degradation behavior.

2.4. *In vitro* degradation and release behaviour

The degradation experiments were conducted in a constant temperature oscillating incubator (SHA-C, China). Firstly, CPC/α-KG were prepared by mixing α-KG polyester microspheres with CPC at mass ratios of 0 : 10 (0 wt% α-KG), 2.5 : 97.5 (2.5 wt% α-KG), 5 : 95 (5 wt% α-KG), and 10 : 90 (10 wt% α-KG), using a turbula powder mixer at 50 rpm for 30 minutes. The blended composite powder was mixed with a curing liquid (0.25 mol L^{-1} NaH_2PO_4 solution) at a powder-to-liquid ratio (P/L) of 2 : 5 (g mL^{-1}). The resulting paste was immediately injected into cylindrical molds (3 mm diameter × 2 mm thickness) and cured at 25 °C with 50% humidity for 24 hours to fabricate standardized CPC/α-KG samples. Subsequently, the samples were air-dried in a ventilated environment for 24 h until reaching constant weight. The initial dry weight of each sample was recorded as M_0. The cured materials were immersed in 0.05 M Tris-HCl buffer with a liquid–solid ratio of 20 mL g^{-1}. The extract solution was replaced every two days, and the experiments were conducted on days 1, 7, 14, 21, 28, 35, 42, 49, and 56, respectively. At different time points, it was removed and dried naturally in a ventilated area and weighed as M_1. Subsequently, replacement extracts were collected at the aforementioned time points to measure the α-KG concentration using high-performance liquid chromatography (Agilent Technologies, USA). The released α-KG in the replacement buffer was quantified using a HPLC system (Agilent 1260, USA) equipped with a ZORBAX SB-C18 column (4.6 × 250 mm, 5 μm; Agilent Technologies, USA). The column temperature was maintained at 25 °C, and the mobile phase consisted of acetonitrile/0.1% phosphoric acid aqueous solution (20 : 80, v/v) delivered at a flow rate of 1.0 mL min^{-1}. Detection was performed at 210 nm with an injection volume of 20 μL. A standard curve was established using α-KG (⩾98% purity, Macklin Biochemical, China) at gradient concentrations (0.5, 1, 2, 5, 10, and 25 μg mL^{-1}), and their peak areas were measured by HPLC. A linear regression equation was derived by plotting peak area (*y*-axis) against concentration (*x*-axis). The α-KG concentration was calculated based on the regression equation. The degradation rate can be calculated *via* the following formula:

$$\text{Degradation (\%)} = M_1/M_0 \times 100\% \quad (1)$$

where M_1 and M_0 respectively represent the final weight at a given time point and the starting weight.

2.5. Biosecurity

BMSCs (1×10^4 per well) were incubated with a-KG composites in 24-well plates for 1 and 3 days to assess the cytocompatibility of the hydrogels. Following a rinse with PBS (BI, USA), the cells were stained with calcein-AM/propidium iodide staining solution for 30 minutes, after which they were imaged with a fluorescence microscope (DMI4000, Germany). The Cell Counting Kit-8 (CCK-8, Biosharp, China) was applied to detect the proliferation of BMSCs. In brief, BMSCs (1×10^4 per well) were cultured with a-KG in 24-well plates for 1 and 3 days, after which the medium was changed to 10% CCK-8 solution and cultured for another 2 h. Absorbance was then quantified *via* a microplate reader (Thermo, USA).

Whole blood from healthy individuals was collected using ethylenediaminetetraacetic acid (EDTA) as an anticoagulant and diluted with phosphate-buffered saline (PBS) at a ratio of 4 : 5. Subsequently, the bone cement samples were immersed into PBS for 30 minutes at 37 °C. The positive and negative control samples were prepared by immersing 3 mL of dH_2O and PBS, respectively. Subsequently, 0.3 mL of the diluted whole blood sample was added and incubated at 37 °C for one hour. Following a 5-minute centrifugation of the samples at 3000 rpm, the supernatant was removed and the OD was detected at 545 nm.

The hemolysis rate (HR) was determined based on the following formula:

$$HR\ (\%) = (OD_s - OD_n)/(OD_p - OD_n) \times 100\% \quad (2)$$

In this equation, OD_s, OD_p, and OD_n correspond to the OD values of the experimental samples, positive, negative control samples, respectively.

2.6. *In vitro* antioxidant and anti-inflammatory assays

Following a 24-hour α-KG pretreatment, BMSCs were subjected to 100 μM H_2O_2 for four hours. The generation of ROS within the cells was evaluated through the simulation of oxidative stress. Subsequently, the cells were washed three times with PBS. Then, they were cultured with 200 μL of DCFH-DA for 0.5 h at 37 °C without light, after which they were imaged using a fluorescence microscope. Following the extraction of RNA using a total RNA extraction kit, cDNA was produced using a PrimeScript™ kit (Takara, Japan). Antioxidant-related genes, such as SOD and catalase (CAT), were then analyzed using quantitative polymerase chain reaction (qPCR) with an ABI Prism 7000 (Thermo, USA) and Ex Taq II (Takara, Japan), with the use of appropriate primers (Table S1, ESI†). Subsequently, the antioxidant-related genes SOD and CAT were subjected to qPCR analysis, along with appropriate primers (Table S1, ESI†). RAW 264.7 cells were plated in 6-well plates and treated with α-KG for three days. Following this, RNA was extracted *via* relevant Extraction Kit for subsequent qPCR analysis of pro-inflammatory-related genes, such as IL-1, IL-6, TNF-α.

2.7. *In vitro* osteogenesis

BMSCs were seeded at 2×10^5 per well in 24-well plates on the composite surface and cultured with osteoblasts. Culture medium (α-MEM medium added 10% ethyl acetate). Osteogenic differentiation medium:[20] culture medium (α-MEM + 10% FBS + 1% penicillin/streptomycin) supplemented with 50 μM ascorbic acid, 10 mM β-glycerophosphate, and 100 nM dexamethasone. Cells were cultured with culture medium for 7 and 14 days. Cells were fixed for 20 min and then stained with BCIP/NBT acid-fast stain. Cells were then stained with a BCIP/NBT alkaline phosphatase (ALP) chromogenic kit and ALP activity was assessed *via* an ALP assay kit. Absorbance was recorded using a microplate reader. Similarly, cells on microtiter plates were stained with 0.1% alizarin red staining (ARS) solution on days 7 and 14. Cells were stained with ARS solution.

On day 7, the cells were digested with trypsin, and total mRNA and total protein were extracted separately. mRNA was used for q-PCR to measure the mRNA expression of the osteogenesis-related genes ALP, BSP, OPN, and RUNX2. Primers were presented in Table S1 (ESI†). The extracted total protein was used for western blotting to analyze the protein expression levels of ALP, BSP, OPN, and RUNX2.

2.8. Repair of osteoporotic bone defects

An osteoporotic model was established in SD rats following previously described methods,[21] with approval from the relevant Animal Research Committee. All procedures were conducted following the international animal welfare standards. After general anesthesia and disinfection, the femoral condyles were exposed by sequential tissue dissection. A 3 mm diameter defect was created in each condyle *via* a ring drill, and the defects were filled with various bone cements. The experimental groups included: control, CPC, and α-KG, with 10 rats per group. At 4 and 8 weeks, rats were euthanized, and the femurs from the implant side were harvested, dehydrated, and fixed. Samples were scanned through a Micro-CT scanner at predefined time points. The area of interest (AOI) was defined as a 3 mm diameter and 2 mm height defect. The mean bone mineral density (BMD) of the AOI was analyzed using Scanco medical software, and the bone volume fraction (BV/TV) was determined *via* the ratio of bone volume to total volume within the AOI. The samples were then stained *via* H&E, Masson's trichrome, and subjected to RUNX2 immunohistochemical staining to evaluate the expression of osteogenic markers.

2.9. Mechanism of action of CPC/α-KG in promoting bone repair capacity

On the third postoperative day, the implanted bone cement was removed by digestion and cultured in 10% FBS medium for 24 h. The cells on the bone cement surface were then digested with trypsin and centrifuged to collect the cells for total RNA extraction. The extracted mRNA was used for subsequent transcriptome sequencing. Differential analysis was performed using the MSstats software package, followed by functional analysis of the differential genes. Western blotting was used to detect p-P110 and p-AKT protein expression levels.

2.10. Statistical analysis

All data were expressed as mean ± SD. Group comparisons were conducted *via* one-way ANOVA and the SNK *post hoc* test. The statistical analysis was conducted using SPSS 21 software, and the judgement criteria was set as $P < 0.05$.

3. Results

3.1. α-KG preparation and characterization

3.1.1. Preparation and detection of α-KG polyester microspheres. The α-KG polyester was obtained through a reaction between α-KG and 1,10-decanediol in a 1 : 1 equimolar ratio (Fig. 1(A)). As illustrated in Fig. 1(B), Fourier transform infrared spectroscopy revealed the presence of characteristic C–O–C bond peaks at wavelengths between 1000 and 1500 cm^{-1}, confirming the successful synthesis of α-KG polyester. Subsequently, a wet gel precipitate was isolated from the α-KG polyester gel solution to obtain α-KG polyester microspheres. The generation of the microspheres was proved by XRD analysis. As illustrated in Fig. 1(C), a distinctive diffraction peak emerged at $2\theta = 22°$, indicative of α-KG as the predominant phase within the material. The morphology of the α-KG polyester microspheres was observed *via* SEM. As illustrated in Fig. 1(D), the microspheres exhibited a circular morphology with a smooth surface.

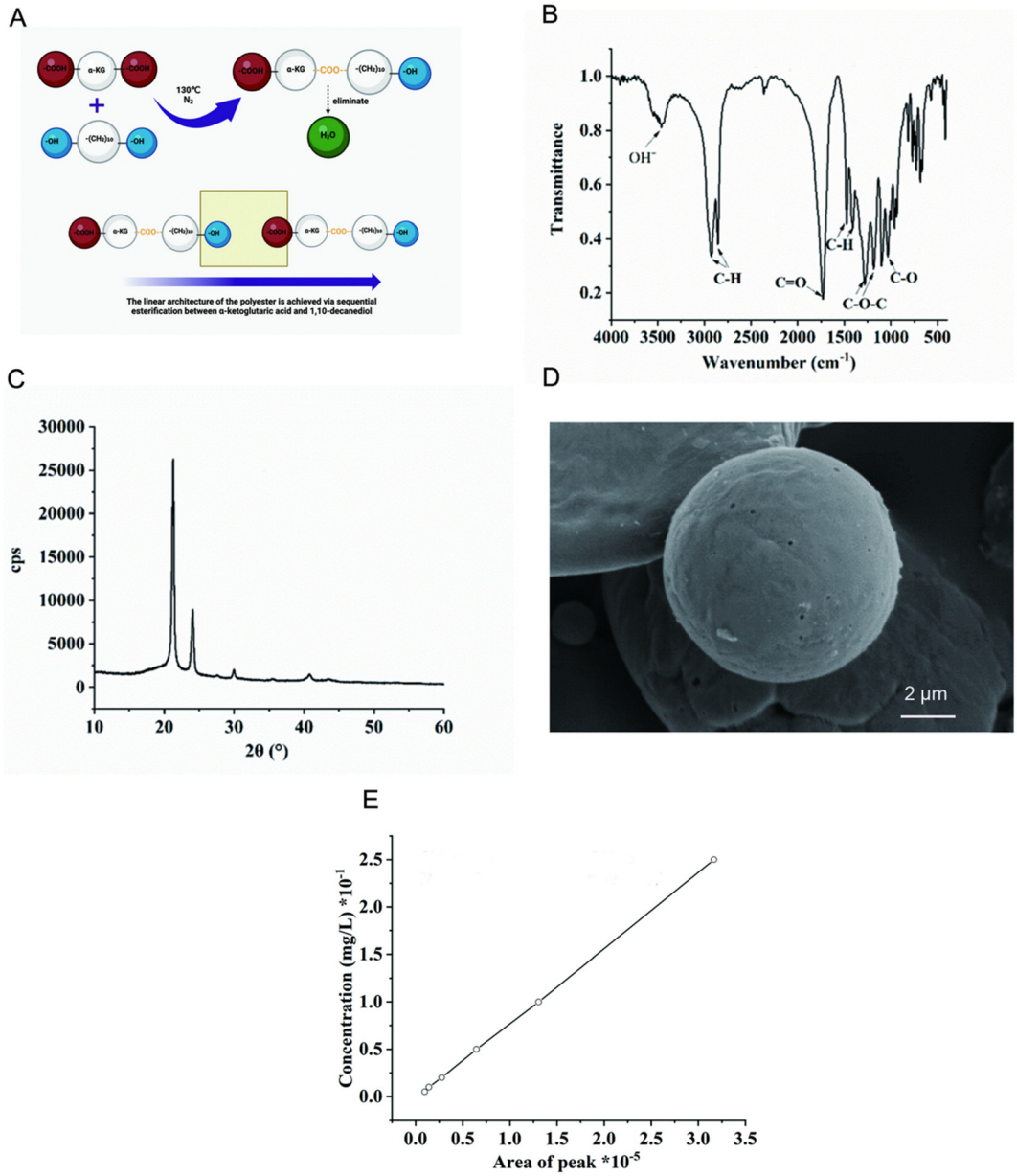

Fig. 1 Characterization of α-KG polyester microspheres. (A) Polyester formation process. (B) Fourier transform infrared spectroscopy for α-KG Polyester Microspheres. (C) XRD analysis. (D) SEM. (E) The α-KG release standard curve. (E) Schematic diagram of the synthesis of α-KG Polyester.

Furthermore, the total area of microspheres at varying concentration ratios was quantified, revealing a linear correlation between the concentration ratio and the microsphere area (Fig. 1(E)). These findings suggest that the synthesized α-KG polyester microspheres possess a uniform structure and are well-suited for medical applications.

3.1.2. Structure and characterization of CPC/α-KG. The CPC powder was obtained by mixing α-tricalcium triphosphate (α-TCP) powder and sodium dihydrogen phosphate (DCPA, NaH_2PO_4) powder in a molar ratio of 1.5 : 1. The aim of this investigation is to ascertain the optimal ratio of α-KG microspheres to CPC. Bone cement containing varying mass ratios of α-KG (0%, 10%, 20%, and 30%) was formulated. The composition of the bone cement in each group was analyzed by XRD (Fig. 2(A)). The characteristic diffraction wave peak of α-KG microspheres was observed at $2\theta = 22^{\circ}$. Subsequently, the beginning and end setting times of the various bone cements were recorded. It was observed that when the concentration of α-KG microspheres exceeded 10%, the beginning and end setting times of the bone cement were prolonged in comparison to the control group (Fig. 2(B)). Consequently, bone cement containing 2.5 wt%, 5 wt%, and 10 wt% α-KG microspheres were constructed for subsequent studies 10%.

SEM was employed to examine the distribution of α-KG microspheres with varying concentrations in the bone cement. As illustrated in Fig. 2(C), the α-KG microspheres within each

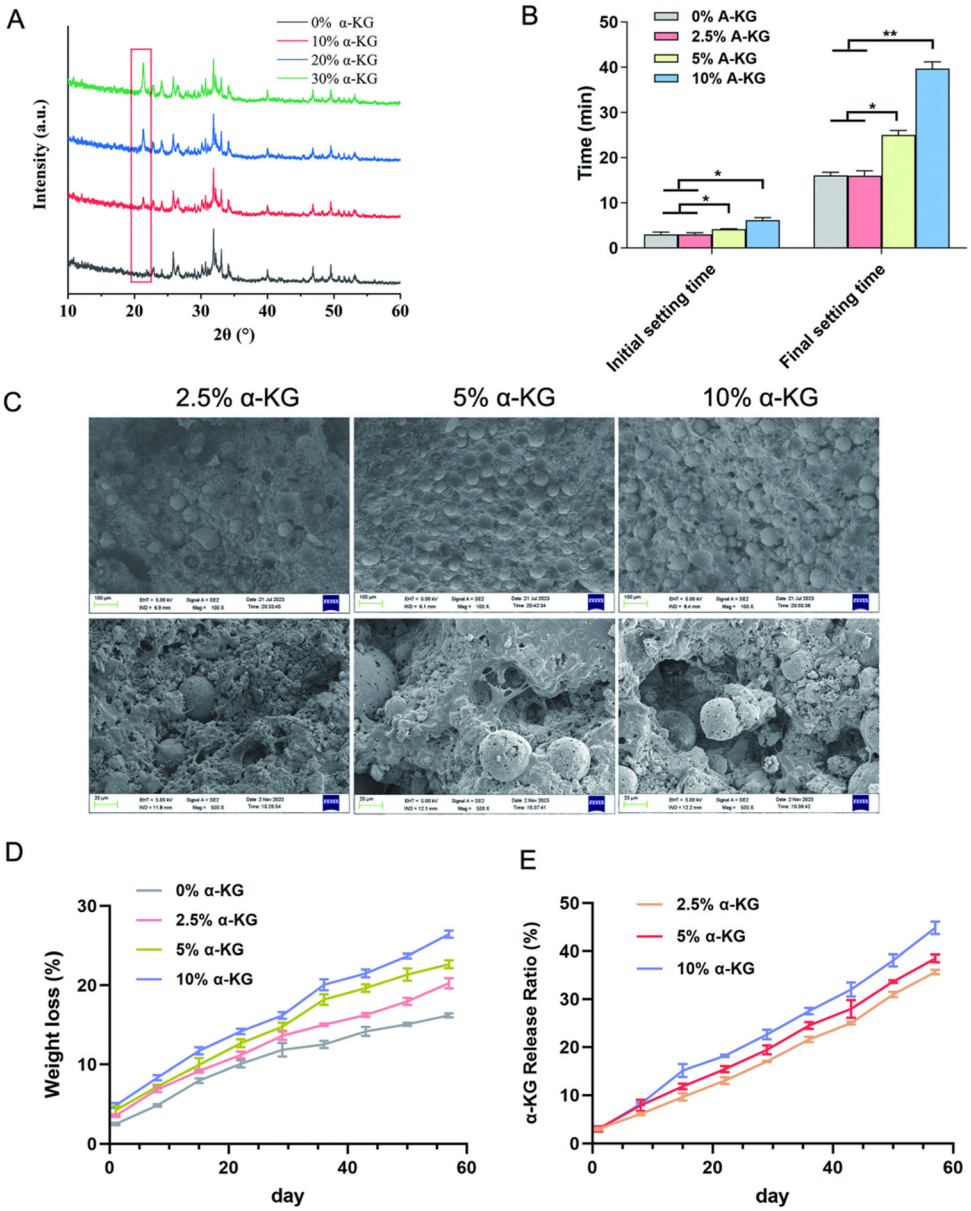

Fig. 2 Characterization of the CPC/α-KG. (A) XRD analysis. (B) Initial and final setting times of the CPC/α-KG. (C) SEM of the CPC/α-KG. (D) Degradation curve of the CPC/α-KG *in vitro*. (E) α-KG release curves of bone cement composed of 2.5%, 5%, and 10 wt% α-KG microspheres. Data are presented as mean ± SD (n = 3); *$p < 0.05$, **$p < 0.01$, ***$p < 0.001$.

group exhibited uniform dispersion within the bone cement structure. To reveal the effect of microsphere incorporation on bone cement biodegradation, the degradation of bone cement with different concentrations of microspheres was examined. As shown in Fig. 2(D), the degradation of bone cement increased in line with the concentration of microspheres. The highest rate of degradation was achieved with 10 wt% α-KG. This phenomenon may be attributed to the hollow structure of the microspheres, which, upon degradation, facilitate the formation of a porous structure within the bone cement. This, in turn, increases the void ratio of the CPC, thereby accelerating the degradation of the bone cement. Consequently, this results in the accelerated release of α-KG and an enhanced osteogenic microenvironment.

As illustrated in Fig. 2(E), bone cement comprising 2.5 wt%, 5 wt%, and 10 wt% α-KG microspheres demonstrated the capacity to release α-KG in a sustained manner. The rate of α-KG release exhibited a discernible acceleration with the augmentation of microsphere content in the bone cement. The degradation of microspheres and the formation of pores within the bone cement further accelerated the degradation of the bone cement.

Comparative analysis of mechanical properties between CPC and α-KG groups revealed distinct performance characteristics. Stress–strain curves demonstrated that the CPC group exhibited consistently higher stress values than the α-KG group (Fig. S1A, ESI†), indicating marginally inferior mechanical strength to the CPC in the α-KG group. This trend was further

confirmed by compressive modulus analysis, where the CPC group showed superior compressive modulus values suggesting enhanced resistance to deformation under axial loading (Fig. S1B, ESI†). Stress variations in the low-strain regime showed that CPC specimens generated higher stress responses during initial loading phases (Fig. S1C, ESI†). Collectively, these findings indicate that while the α-KG group displayed reduced overall mechanical performance compared to CPC, its elastic modulus range (3000–4000 MPa) demonstrated closer alignment with the documented modulus range of human cancellous bone (10–3000 MPa)[22]. This suggests potential biomechanical compatibility advantages for α-KG in bone defect repair applications, requiring modulus matching with native tissue.

As illustrated in Fig. S1D (ESI†), both groups exhibited a progressive reduction in mass over time, which was indicative of material degradation or erosion within the liquid medium. Compared to the CPC group, the α-KG group demonstrated a more pronounced mass loss trajectory, suggesting a higher degradation rate associated with α-KG incorporation. Fig. S1E (ESI†) further revealed that the erosion rates of both groups increased with prolonged exposure, displaying broadly similar temporal trends. However, the α-KG group exhibited marginally elevated erosion rates at specific intervals, further supporting the hypothesis that α-KG microspheres accelerates material degradation. Collectively, these findings demonstrate that α-KG microspheres significantly alters the degradation behavior of the material, rendering it more susceptible to environmental factors such as fluid shear stress and hydrolytic dissolution.

In conclusion, the incorporation of α-KG polyester microspheres into CPC results in a tunable pore degradation rate and an enhanced degradation performance of the traditional CPC. Concurrently, the degradation of bone cement facilitates the release of α-KG, which can further regulate the osteogenic microenvironment of osteoporotic bone defects. The α-KG polyester microsphere CPC demonstrates significant potential for application.

3.2. Biosecurity

In vitro biosafety assessments of α-KG were conducted using live–dead staining, CCK8, and hemolysis assays. Initially, live/dead staining was employed to evaluate its biocompatibility (Fig. 3(A)). Live BMSCs were stained with green fluorescence (calcineurin-AM), and dead BMSCs were stained with red fluorescence (PI). At day 1 and day 3, there was no evidence of significant cell death, and cell proliferation was comparable to the control group, indicating that α-KG did not exhibit substantial toxicity. The subsequent CCK-8 results were in accordance with the live–dead staining results (Fig. 3(B)). Furthermore, the hemolysis rate serves as an additional index for evaluating the biocompatibility of biomaterials. The results of the hemolysis experiments are presented in Fig. 3(C).

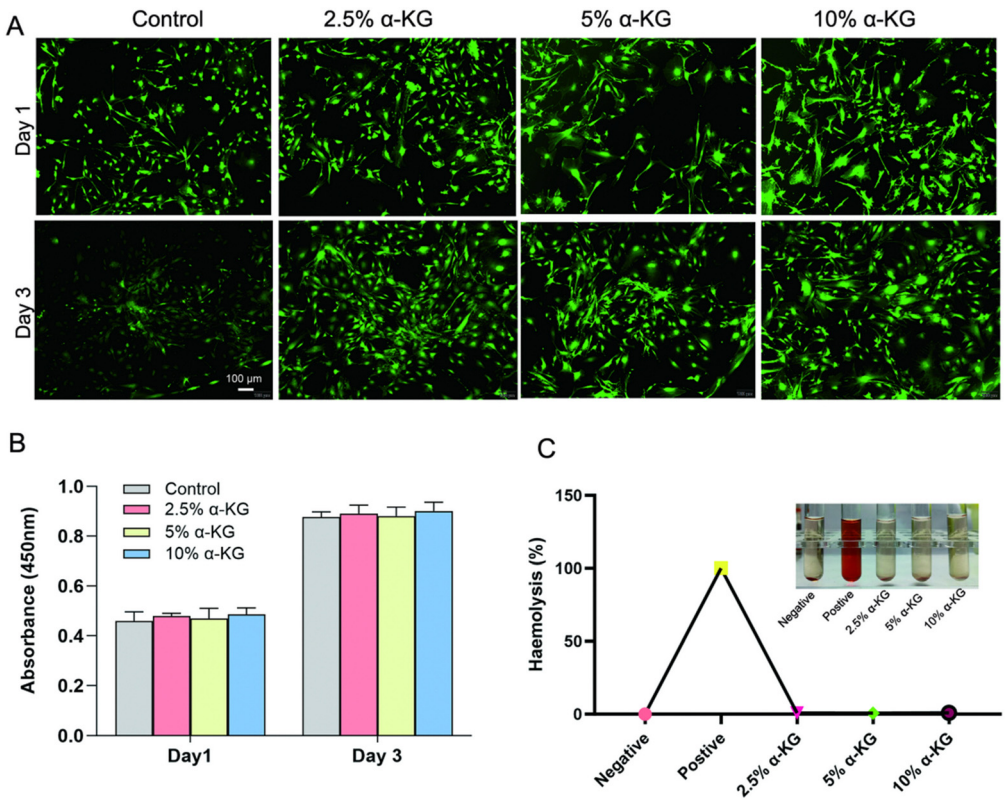

Fig. 3 Diosafety assessments *In vitro*. (A) Fluorescence images of BMSCs incubated with different CPC/α-KG for 1 and 3 days, respectively. Scale bar = 200 μm. (B) CCK-8 assay for BMSCs cultured with different CPC/α-KG for 1 and 3 days, respectively. (C) Hemolysis of different CPC/α-KG *in vitro*. Data are presented as mean ± SD (n = 3); *p < 0.05, **p < 0.01, ***p < 0.001.

The supernatant of the positive control group exhibited a reddish hue due to the rupture of erythrocytes, whereas the supernatant of the negative control group and α-KG group was still clear. The calculated hemolysis rate was less than 5%, indicating that all of the bone cements demonstrated favorable biocompatibility. Accordingly, 10 wt% α-KG was chosen for further experimental investigation.

3.3. Antioxidant activity *in vitro*

An excessive accumulation of ROS impairs the proliferation and differentiation of osteoblasts, which in turn affects the fracture healing process. The aim of the present research was to evaluate the antioxidant performance of α-KG polyester microspheres in CPC *in vitro*. Initially, DCFH-DA was employed to quantify intracellular ROS levels in BMSCs subjected to hydrogen peroxide stress conditions. As illustrated in Fig. 4(A), a substantial fluorescence signal was observed in the control and CPC groups, which exhibited the lowest α-KG fluorescence. This indicates that the incorporation of α-KG microspheres into CPC can augment the anti-ROS capacity. Additionally, the effect of material degradation products on the expression of the enzymes SOD and CAT in BMSCs was examined using qPCR. The results are presented in Fig. 4(B) and (C). According to the comparison result, the α-KG group showed obvious upregulation in mRNA expression of the SOD and CAT genes. These findings suggest that the incorporation of α-KG polyester microspheres into CPC enhances the antioxidant properties of CPC.

3.4. Anti-inflammatory *in vitro*

Repair of bone defects is dependent on osteogenic differentiation of bone marrow MSCs and excessive inflammation impairs this process. RAW264.7 was used to assess the anti-inflammatory effects of α-KG. The expression of inflammation-related factors

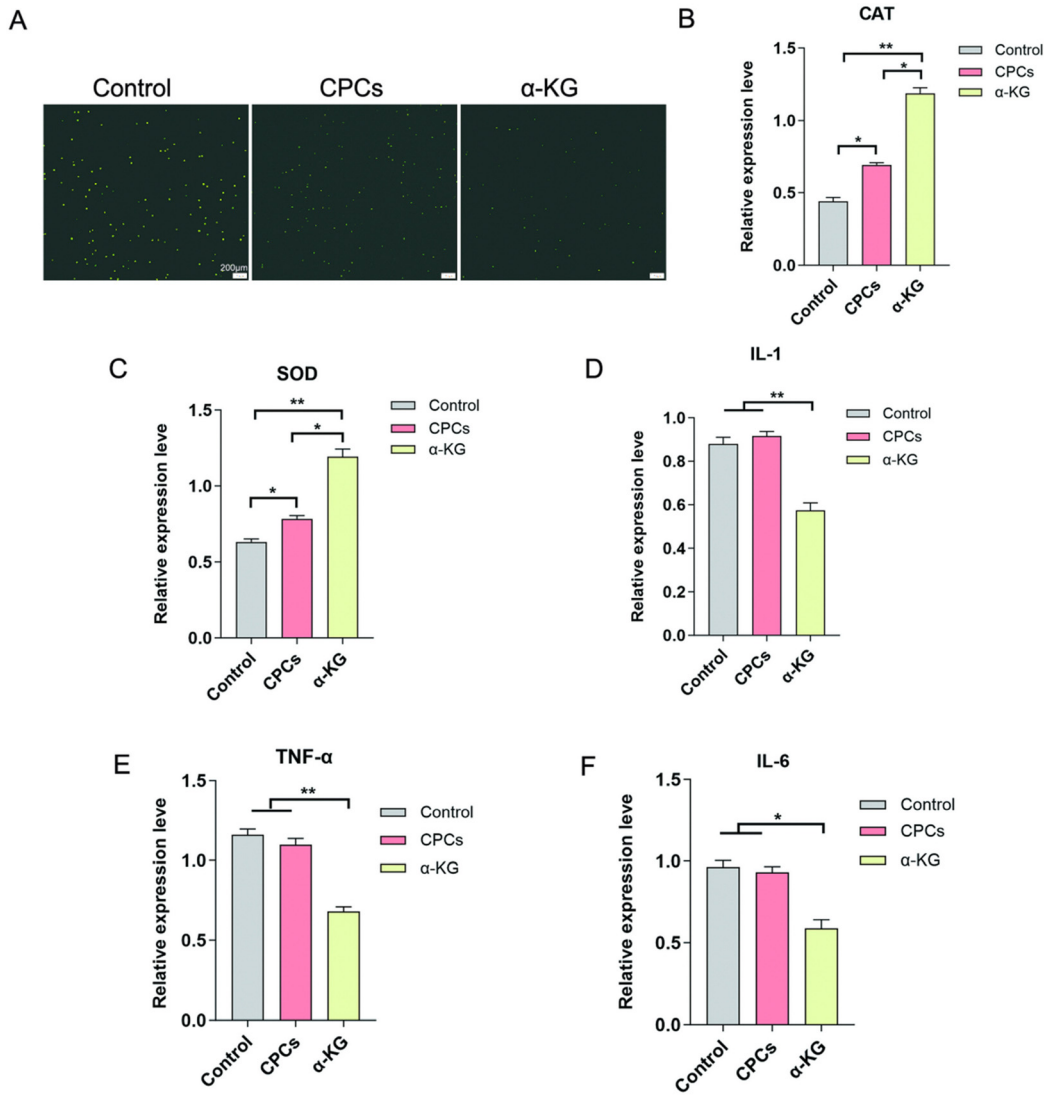

Fig. 4 Anti-inflammatory and Antioxidant activity *in vitro*. (A) Representative fluorescence images of total intracellular ROS (DCFH-DA) of BMSCs after incubation with α-KG for 24 h and further exposure to H_2O_2 for 4 h. The scale bar is 200 μm (B) Relative expression of CAT and SOD in culture with α-KG. (C)–(F) Relative expression of IL-1, TNF-α and IL-6 in culture with α-KG. Data are presented as mean ± SD (n = 3); *$p < 0.05$, **$p < 0.01$, ***$p < 0.001$.

was determined by q-PCR. As shown in Fig. 4(D)–(F), IL-1, IL-6, TNF-α mRNA expression was obviously lower in the α-KG group compared to that in the control and CPC groups. This indicates that the addition of α-KG polyester microspheres to CPC enhanced the anti-inflammatory capacity. In addition, excessive ROS or inflammation induces senescence in BMSCs, which affects osteogenic differentiation.

3.5. Osteogenesis *in vitro*

The impact of α-KG on osteogenic differentiation was investigated through the utilization of alizarin staining, ALP staining, and q-PCR.

ARS was employed to assess the formation of inorganic calcium deposits, a marker of mineralization and osteogenesis. Mature inorganic calcium was stained red; the darker the color, the greater the number of surface calcium salts deposited. As illustrated in Fig. 5(A), calcium salt deposition on bone cement increased from 7 to 14 days. The darkest staining in the 10 wt% α-KG group indicates the highest calcium salt deposition.

ALP is a commonly used indicator for evaluating the beginning phase of osteogenic differentiation. The shade of blue-purple observed in ALP staining was found to be positively related to the degree of cell differentiation. The 10 wt% α-KG group exhibited the darkest staining on days 7 and 14 (Fig. 5(B)). Subsequently, ALP activity was quantified. As illustrated in Fig. 5(C), the 10 wt% α-KG group demonstrated the highest ALP activity, which was consistent with the staining results.

Furthermore, tube-forming-related gene expression was quantified by qPCR. As illustrated in Fig. 5(D) and (E), the level of tube-forming-related genes, including ALP, RUNX2, OPN, and BSP, was markedly elevated compared with the control group, with the 10 wt% α-KG group exhibiting the most pronounced increase. Subsequently, the protein expression of ALP, RUNX2, OPN, and BSP was further verified by western blot

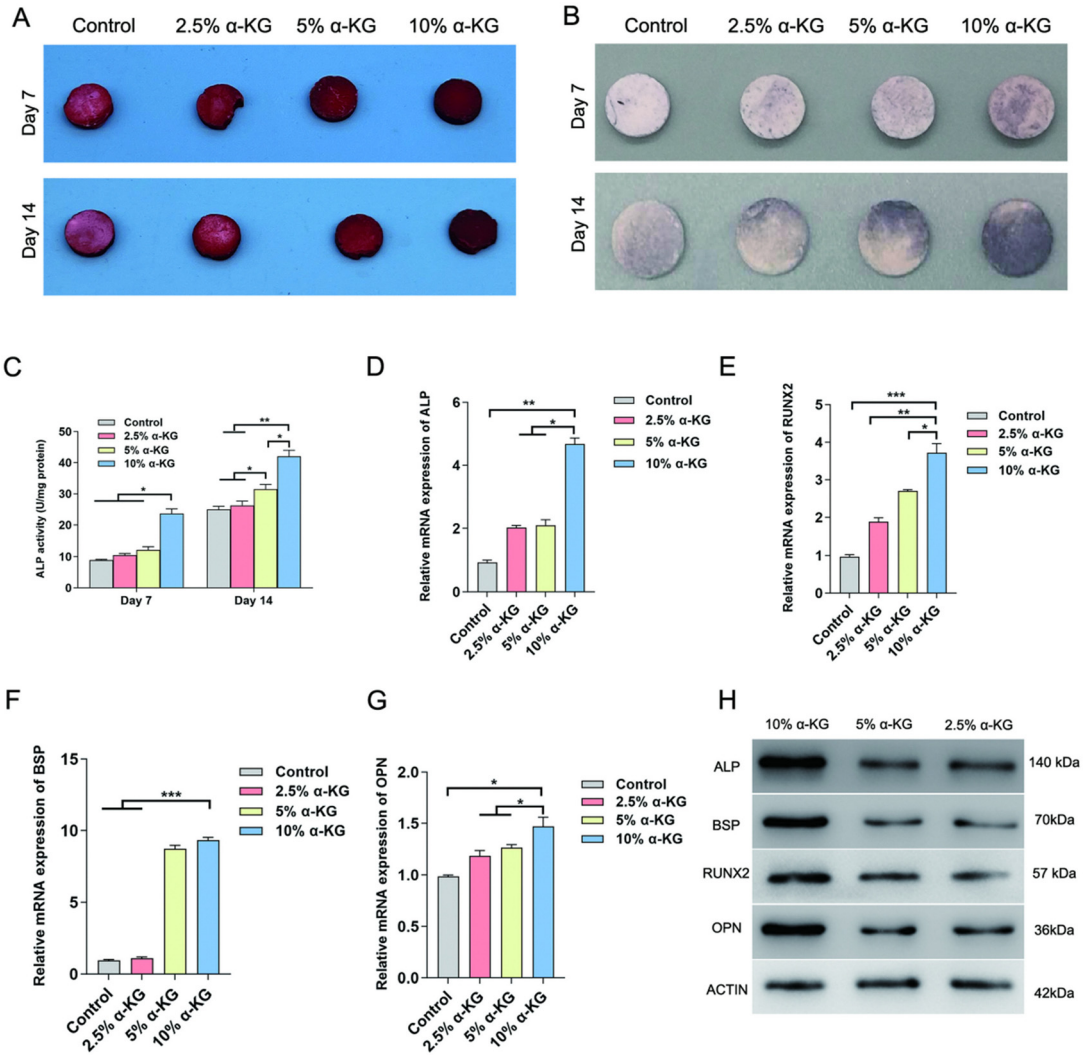

Fig. 5 The osteogenic effect of α-KG *in vitro*. (A) ARS staining. (B) ALP staining. (C) Quantitative ALP activity. (D)–(G) RT-qPCR analysis of osteogenesis-related genes (ALP, RUNX2, BSP, and OPN) in different α-KG. (H) Western blot evaluation of osteogenic protein expression. $N = 3$, $^{*}P < 0.05$, $^{**}P < 0.01$, $^{***}P < 0.001$.

analysis. As illustrated in Fig. 5(F), the results demonstrated that the level of osteogenesis-related proteins was up-regulated in all groups. Furthermore, the protein expression was more significant with an increase in α-KG content. These findings suggest that the introduction of α-KG polyester microspheres into CPC significantly enhanced its bone-enhancing effect.

3.6. *In vivo* assessment of the repair of bone tissue

An osteoporotic rat femoral defect model was applied to evaluate the influence of bone cement on bone defect repair. The experiment was conducted with three distinct groups: the control group, the CPC group (CPC), and the CPC/α-KG group (α-KG). The bone formation of each group at four and eight weeks was assessed using micro-CT. The results are presented in Fig. 6(A), wherein the green color denotes new bone formation. The α-KG group exhibited the highest amount of new bone at weeks 4 and 8, which was significantly greater than that observed in the CPC group and blank control group. As illustrated in Fig. 6(B) ad (C), the bone volume fraction and bone density were markedly higher in the α-KG group compared to the CPC and the control groups. This finding aligns with the outcomes of the *in vitro* experiments. Consequently, it can be inferred that the incorporation of α-KG polyester microspheres can enhance the osteogenic properties of CPC and augment osteoinductivity.

3.7. Tissue staining

Furthermore, the presence of inflammation and new bone formation was discerned by the utilization of H&E and Masson's staining methods. As illustrated in Fig. 7(A), the presence of inflammation and fibrous tissue was observed in the region of bone defects across all experimental groups. The control group and the CPC group showed substantial inflammatory cell infiltration, whereas the α-KG group demonstrated a relatively minimal inflammatory response. Additionally, the α-KG group displayed a greater prevalence of newly formed bone tissue staining blue (Fig. 7(B)). In the Masson staining sections, by 8 weeks, although collagen fibers could still be observed, their quantity and distribution range were reduced compared those at 4 weeks, with a decrease in the proportion of blue-stained collagen fiber areas and an increase in the mineralized areas representing bone tissue. RUNX2 immunohistochemical staining further indicated that the

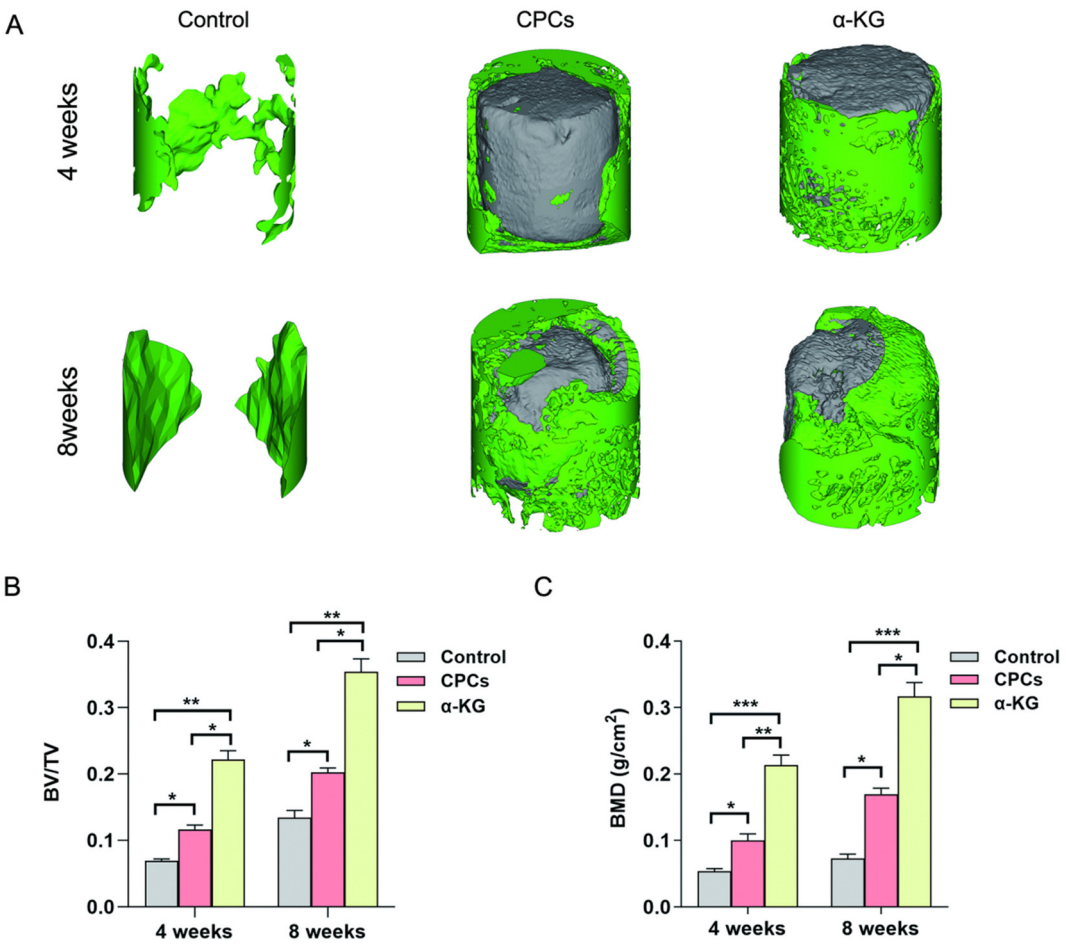

Fig. 6 Evaluation of *in situ* bone regeneration. (A) Microscopic CT imaging of femoral defects in rats with stent implantation at 4 and 8 weeks, with green areas indicating new bone. (B) and (C) Quantitative analysis of BV/TV and BMD at 4 and 8 weeks post-implantation. $N = 5$, $^{*}P < 0.05$, $^{**}P < 0.01$, $^{***}P < 0.001$.

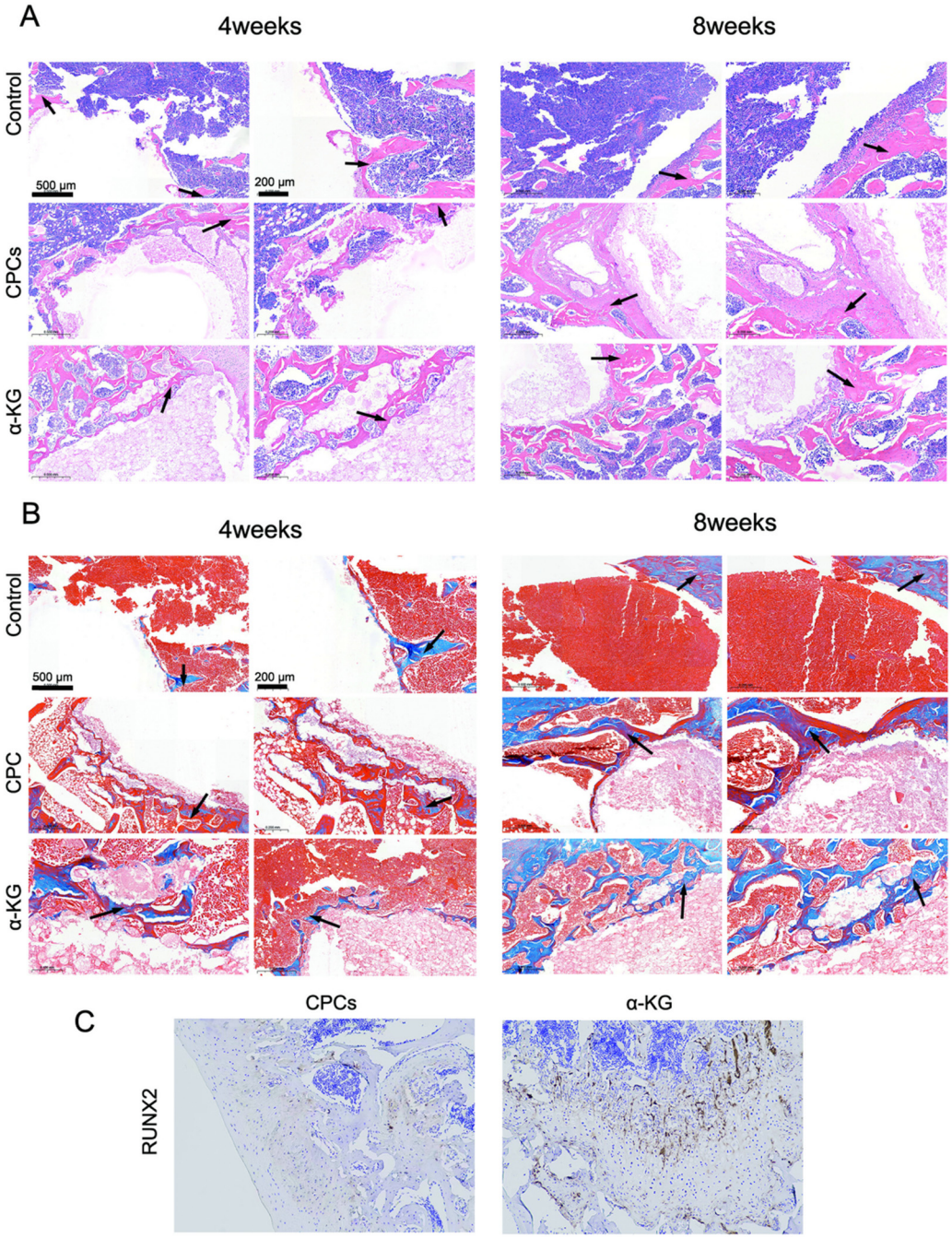

Fig. 7 Histological examination *in vivo*. (A) H&E Staining. (B) Masson's trichrome staining. The newly formed skeleton is indicated by the arrow. (C) Immunohistochemistry of RUNX2.

α-KG group had obviously higher levels of RUNX2, a key transcription factor in osteogenesis, compared to the control and CPC group. This indicates enhanced osteogenic activity in the α-KG-treated bone defect regions (Fig. 7(C)). Moreover, it suggests that the release of α-KG may effectively reduce inflammation, oxidative stress, and excessive fibrosis, while promoting RUNX2 expression, enhancing osteogenic activity, and facilitating the transition from collagen fiber deposition to mineralized bone tissue formation in the bone defect regions.

3.8. Mechanism of α-KG bone cement osteogenic microenvironment regulation

To investigate the mechanism by which α-KG bone cement regulates osteoporotic bone defects, bone cements were implanted into the femoral defect site of rats and collected on day 3. This yielded three CPC and three α-KGs, respectively. The cells on the bone cements surface were digested, and nucleic acids were extracted for transcriptological sequencing. Fig. 8(A) and (B) illustrate the volcano map and gene expression

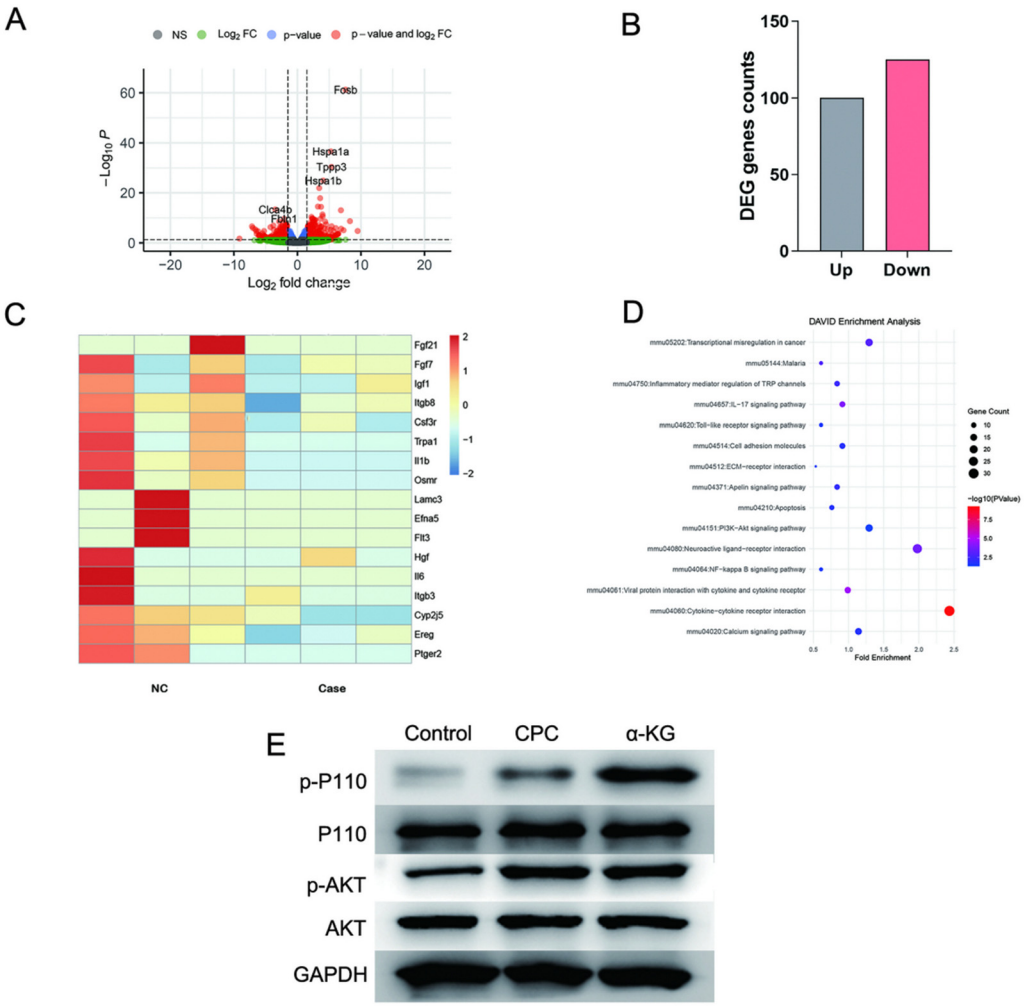

Fig. 8 Regulatory mechanism of local osteogenic microenvironment in α-KG. (A) Volcano map of differentially expressed genes. (B) Histogram displaying the number of differentially expressed genes. (C) Heatmap of the differentially expressed mRNAs treated with α-KG or in the N.C. group (D) KEGG pathway analysis of differentially expressed genes. (E) Western blot detection of expression levels of *PI3K/AKT* pathway proteins.

heat map, respectively. Fig. 8(C) depicts the number of up- and down-regulated genes. Fig. 8(D) shows the KEGG pathway enrichment analysis showing enrichment of the *PI3K/AKT* pathway. This pathway is associated with promoting osteogenic differentiation, inhibiting the inflammatory response and reducing oxidative stress.

PI3K/AKT pathway protein expression levels were verified by WB. As shown in Fig. 8(E), the phosphorylated protein expression of P110 and AKT was most prominent in the α-KG group.

This indicates that α-KG exerts an influence on inflammation, oxidative stress, and regulating the osteogenic environment *via* the *PI3K/AKT* signaling pathway, which obviously regulates the repair of osteoporotic bone defects.

4. Discussion

In this study, α-KG was first synthesized into α-KG polyester which was then formed into α-KG polyester microspheres. Using α-KG as the reference substance, these microspheres were prepared and characterized. Subsequently, they were incorporated into CPC structures. The incorporation of α-KG polyester microspheres led to a faster degradation rate of the CPC, and their degradation increased the porosity of the CPC. Concurrently, α-KG, with its anti-inflammatory, antioxidant, and bone-enhancing abilities, improved the osteogenic microenvironment of osteoporotic bone defects and facilitated *in situ* osteogenesis within the bone cement. In essence, the degradation of the α-KG polyester microsphere releases α-KG while modulating the degradation rate of the bone cement (Fig. 1 and 2), which meets the need for the modification of calcium phosphate bone cements.

The CPC/α-KG elicited dual material-biological effects that synergistically enhanced osteogenic capacity. Material-wise, similar to the effects previously observed with citric acid[23] and phytic acid[24] modified cements, α-KG prolongs the setting time of CPC by enhancing the negative zeta potential (electrostatic repulsion) of cement particles and dynamically chelating

calcium ions, while maintaining material strength due to optimized crystallization densification. Concurrently, the degradation of α-KG microspheres within the CPC matrix created interconnected pores with porosity positively correlating to α-KG content, a phenomenon consistent with PLGA/CPC composites.[25,26] Biologically, the healing process of osteoporotic fractures is associated with delayed healing and a poor osteogenic microenvironment under pathological conditions. Excessive accumulation of ROS and inflammation are key pathological factors in osteoporosis, which result in an imbalance between bone formation and loss. The ''seed and soil'' hypothesis[27] suggests that simultaneous enhancement of seed quality and soil environment can improve the therapeutic outcome of osteoporotic bone defects. α-KG, as an antioxidant, was very important in ROS scavenging.[28] *In vitro* experiments demonstrated that CPC/α-KG was capable of scavenging ROS produced by BMSCs and inhibiting the expression of anti-inflammatory factors (Fig. 4). This aligns with recent studies on the osteogenic mechanisms of α-KG.[29,30] Consequently, this process facilitated the creation of an optimal environment for bone regeneration, leading to the upregulation of osteogenic genes such as ALP, BSP, OPN, and RUNX2 (Fig. 5). In the SD rat osteoporotic femur model, calcium phosphate bone cements incorporating α-KG polyester microspheres exhibited remarkable osteogenic potential and anti-inflammatory properties (Fig. 6 and 7). Transcriptional sequencing also revealed that the bone cement was enriched in osteogenic, antioxidative, and anti-inflammatory signaling pathways. α-KG affects the osteogenic microenvironment of bone tissue *via* the *PI3K/AKT* signaling pathway, which accordingly regulates the repair of osteoporotic bone defects (Fig. 8).

Calcium phosphate cement (CPC), while widely used as a bone repair material,[31] exhibits inherent limitations such as brittleness and inconsistent degradation rates.[32] To address these issues, polymeric modifications of CPC have gained significant momentum in recent years. Materials such as PLGA (poly(lactic-*co*-glycolic acid)),[33–35] PEGS (PEGylated poly),[36,37] and PAAS (sodium polyacrylate)[38] have been incorporated into CPC to enhance its mechanical properties like strength, toughness and adjust setting time to facilitate bone healing. Distinctively, our CPC/α-KG strategy focuses on leveraging the bioactive benefits of α-KG without substantially compromising the intrinsic mechanical advantages of CPC. The sustained release of α-KG from CPC/α-KG not only ameliorates the osteoporotic microenvironment by suppressing osteoclast activity and oxidative stress but also synergistically promotes osteogenesis through metabolic regulation. This dual functionality positions CPC/α-KG as a promising candidate for pathological bone regeneration, particularly in osteoporosis-related defects. Recent advancements in materials for osteoporotic bone repair have shown promising progress, particularly in injectable materials and scaffold materials. Notably, CPC/α-KG demonstrates comparable effects in ameliorating the osteoporotic microenvironment and promoting bone defect healing. In contrast to the injectable hydrogels[39] and bioceramic scaffolds,[40] CPC/α-KG achieves a balance between suitable elastic modulus (3000–4000 MPa) and adaptability to irregular defect geometries.

In summary, the CPC/α-KG composite demonstrates exceptional potential for bone regeneration by synergistically combining controlled degradability and robust osteogenic activity, effectively accelerating bone formation through integrated mechanisms such as anti-inflammatory modulation, antioxidant protection, and optimization of the osteogenic microenvironment. This multifunctional system not only addresses structural and metabolic challenges in bone repair but also highlights its transformative potential for clinical applications in orthopedics and regenerative medicine. However, the underlying molecular mechanisms—such as the metabolic crosstalk between CPC degradation products and cellular energy metabolism, and dynamic immune–microenvironment interactions—require deeper investigation. Further studies should focus on *in vivo* validation of mechanism hypotheses and long-term biocompatibility evaluation to bridge the gap between experimental promise and clinical translation. Addressing these questions will further establish CPC/α-KG as a next-generation bioactive material for bone repair.

5. Conclusion

In summary, we addressed the limitations of slow degradation and limited osteogenesis in calcium phosphate bone cements by incorporating α-KG polyester microspheres. We demonstrated that adjusting the microsphere content allowed us to achieve a suitable setting time and an appropriate degradation rate for the CPC/α-KG. The composites demonstrated robust antioxidant and anti-inflammatory properties *in vitro*, effectively enhancing the osteogenic microenvironment of osteoporotic bone defects. Transcriptional sequencing revealed activation of osteogenic, antioxidative, and anti-inflammatory pathways, with mechanistic validation identifying the *PI3K/AKT* signaling axis as a key driver of α-KG-mediated osteogenesis. The CPC/α-KG elicited dual material-biological effects that synergistically enhanced osteogenic capacity, highlighting its potential to integrate material adaptability with metabolic regulation. This study provides new insights into the construction and clinical utilization of osteoporotic bone defect repair materials by exploring the material–metabolic interplay. These findings enhance the understanding of α-KG's role in bone remodeling and may contribute to the development of biomaterials that better adapt to pathological microenvironments. Additionally, they have potential implications for treating complex skeletal disorders where inflammation, oxidative stress, and impaired healing coexist. To support clinical translation, future studies should focus on validating these mechanisms in physiologically relevant osteoporotic models and establishing standardized biocompatibility protocols, ultimately bridging biomaterial design with clinical applications.

Ethical approval

This study was conducted following approval from the Institutional Animal Care and Use Committee (IACUC) of the Southern

Medical University (no. SYT2024081). All animal procedures adhered to ethical standards and guidelines to ensure humane treatment and minimize suffering.

Author contributions

Zhengyang Kang: conceptualization, formal analysis, methodology, writing – original draft, writing – review & editing. Hui Yang: writing – review & editing, writing – original draft, methodology, investigation, formal analysis, conceptualization. Xinzhi Liang: writing – review & editing, investigation, formal analysis, conceptualization. Bin Wu: formal analysis, writing – review & editing. Dequan Wang: formal analysis, writing – review & editing. Luhui Zhang: formal analysis, writing – review & editing. Denghui Xie: writing – review & editing, writing – original draft, methodology, investigation, formal analysis, conceptualization.

Data availability

All experimental data, including raw images and detailed material characterization datasetsare provided in the manuscript. Additionally, the complete raw datasets have been deposited in the Zenodo repository under DOI: 10.5281/zenodo.15164889.

Conflicts of interest

The authors declare that they have no known competing financial interests or personal relationships that could have appeared to influence the work reported in this paper.

Acknowledgements

The National Natural Science Foundation of China (no. 81974328, 82372358, 82072443 and 82372425), the Natural Science Foundation for Distinguished Young Scholars of Guangdong Province (2022B1515020044) Guangdong Students' Platform for Innovation and Entrepreneurship Training Program (S202312121083), the Science and Technology Program for Medical and Health Projects of Panyu Guangzhou (2023-Z04-043).

References

1 I. Sotornik, Osteoporosis – epidemiology and pathogenesis, *Vnitr. Lek.*, 2016, **62**(Suppl 6), 84–87.
2 Y. Schwarcz, C. Yanover, V. Rouach, S. Luria and I. Goldshtein, Non-osteoporotic fractures are associated with increased risk of subsequent major osteoporotic fractures, *Osteoporosis Int.*, 2024, **35**(10), 1839–1847.
3 J. A. Li, L. Li, T. K. Wu, K. Shi, Z. W. Bei and M. Wang, *et al.*, An Injectable Thermosensitive Hydrogel Containing Resveratrol and Dexamethasone-Loaded Carbonated Hydroxyapatite Microspheres for the Regeneration of Osteoporotic Bone Defects. Small, *Methods*, 2024, **8**(1), 17.
4 X. Liang, X. D. Yang, J. Liu, L. F. Tu, W. X. Wei and H. J. Wang, *et al.*, ROS-scavenging bioactive scaffold orchestrates bone regeneration for osteoporotic bone defect repair, *Composites, Part B*, 2024, **281**, 16.
5 A. H. Schmidt, Autologous bone graft: Is it still the gold standard?, *Injury-Int. J. Care. Inj.*, 2021, **52**, S18–S22.
6 E. García-Gareta, M. J. Coathup and G. W. Blunn, Osteoinduction of bone grafting materials for bone repair and regeneration, *Bone*, 2015, **81**, 112–121.
7 L. M. Ma, S. Cheng, X. F. Ji, Y. Zhou, Y. S. Zhang and Q. T. Li, *et al.*, Immobilizing magnesium ions on 3D printed porous tantalum scaffolds with polydopamine for improved vascularization and osteogenesis, *Mater. Sci. Eng., C*, 2020, **117**, 11.
8 P. Baldwin, D. J. Li, D. A. Auston, H. S. Mir, R. S. Yoon and K. J. Koval, Autograft, Allograft, and Bone Graft Substitutes: Clinical Evidence and Indications for Use in the Setting of Orthopaedic Trauma Surgery, *J Orthop Trauma*, 2019, **33**(4), 203–213.
9 S. S. Leopold, J. J. Jacobs and A. G. Rosenberg, Cancellous allograft in revision total hip arthroplasty: A clinical review, *Clin. Orthop. Relat. Res.*, 2000, **371**, 86–97.
10 Z. Sheikh, S. Najeeb, Z. Khurshid, V. Verma, H. Rashid and M. Glogauer, Biodegradable Materials for Bone Repair and Tissue Engineering Applications, *Materials*, 2015, **8**(9), 5744–5794.
11 L. Deng and Y. Yan, Research status and progress of biomaterials for bone repair and reconstruction, *Chin. J. Repar. Reconstr. Surg.*, 2018, **32**(7), 815–820.
12 J. T. Zhang, W. Z. Liu, V. Schnitzler, F. Tancret and J. M. Bouler, Calcium phosphate cements for bone substitution: Chemistry, handling and mechanical properties, *Acta Biomater.*, 2014, **10**(3), 1035–1049.
13 H. H. K. Xu, P. Wang, L. Wang, C. Y. Bao, Q. M. Chen and M. D. Weir, *et al.*, Calcium phosphate cements for bone engineering and their biological properties, *Bone Res.*, 2017, **5**, 19.
14 J. Jeong, J. H. Kim, J. H. Shim, N. S. Hwang and C. Y. Heo, Bioactive calcium phosphate materials and applications in bone regeneration, *Biomater. Res.*, 2019, **23**(1), 11.
15 A. A. Shahmirzadi, D. Edgar, C. Y. Liao, Y. M. Hsu, M. Lucanic and A. A. Shahmirzadi, *et al.*, Alpha-Ketoglutarate, an Endogenous Metabolite, Extends Lifespan and Compresses Morbidity in Aging Mice, *Cell Metab.*, 2020, **32**(3), 447–456.
16 Y. Wang, P. Deng, Y. Liu, Y. Wu, Y. Chen and Y. Guo, *et al.*, Alpha-ketoglutarate ameliorates age-related osteoporosis *via* regulating histone methylations, *Nat. Commun.*, 2020, **11**(1), 5596.
17 D. G. Barrett and M. N. Yousaf, Poly(triol α-ketoglutarate) as biodegradable, chemoselective, and mechanically tunable elastomers, *Macromolecules*, 2008, **41**(17), 6347–6352.
18 J. L. Mangal, S. Inamdar and A. P. Suresh, Jaggarapu MMCS, Esrafili A, Ng ND, *et al.* Short term, low dose alpha-ketoglutarate based polymeric nanoparticles with methotrexate reverse rheumatoid arthritis symptoms in mice and

modulate T helper cell responses, *Biomater. Sci.*, 2022, **10**(23), 6688–6697.
19 R. P. F. Lanao, S. C. G. Leeuwenburgh, J. G. C. Wolke and J. A. Jansen, Bone response to fast-degrading, injectable calcium phosphate cements containing PLGA microparticles, *Biomaterials*, 2011, **32**(34), 8839–8847.
20 N. Jaiswal, S. E. Haynesworth, A. I. Caplan and S. P. Bruder, Osteogenic differentiation of purified, culture-expanded human mesenchymal stem cells *in vitro*, *J. Cell. Biochem.*, 1997, **64**(2), 295–312.
21 D. N. Kalu, The ovariectomized rat model of postmenopausal bone loss, *Bone Miner.*, 1991, **15**(3), 175–191.
22 E. F. Morgan, G. U. Unnikrisnan and A. I. Hussein, Bone Mechanical Properties in Healthy and Diseased States, *Annu. Rev. Biomed. Eng.*, 2018, **20**, 119–143.
23 S. Sarda, E. Fernández, M. Nilsson, M. Balcells and J. A. Planell, Kinetic study of citric acid influence on calcium phosphate bone cements as water-reducing agent, *J. Biomed. Mater. Res.*, 2002, **61**(4), 653–659.
24 K. Hurle, J. Weichhold, M. Brueckner, U. Gbureck, T. Brueckner and F. Goetz-Neunhoeffer, Hydration mechanism of a calcium phosphate cement modified with phytic acid, *Acta Biomater.*, 2018, **80**, 378–389.
25 P. Cai, S. Lu, J. Yu, L. Xiao, J. Wang and H. Liang, *et al.*, Injectable nanofiber-reinforced bone cement with controlled biodegradability for minimally-invasive bone regeneration, *Bioact. Mater.*, 2023, **21**, 267–283.
26 L. Huang, P. Cai, M. Bian, J. Yu, L. Xiao and S. Lu, *et al.*, Injectable and high-strength PLGA/CPC loaded ALN/MgO bone cement for bone regeneration by facilitating osteogenesis and inhibiting osteoclastogenesis in osteoporotic bone defects, *Mater. Today Bio*, 2024, **26**, 101092.
27 I. J. Fidler, The pathogenesis of cancer metastasis: the 'seed and soil' hypothesis revisited, *Nat. Rev. Cancer*, 2003, **3**(6), 453–458.
28 S. Liu, L. He and K. Yao, The Antioxidative Function of Alpha-Ketoglutarate and Its Applications, *BioMed Res. Int.*, 2018, **2018**, 3408467.
29 L. Liu, W. Zhang, T. Liu, Y. Tan, C. Chen and J. Zhao, *et al.*, The physiological metabolite α-ketoglutarate ameliorates osteoarthritis by regulating mitophagy and oxidative stress, *Redox Biol.*, 2023, **62**, 102663.
30 R. He, Y. Wei, Z. Peng, J. Yang, Z. Zhou and A. Li, *et al.*, α-Ketoglutarate alleviates osteoarthritis by inhibiting ferroptosis *via* the ETV4/SLC7A11/GPX4 signaling pathway, *Cell. Mol. Biol. Lett.*, 2024, **29**(1), 88.
31 Y. Gu, R. Zhuang, X. Xie and Y. Bai, Osteogenic stimulation of human dental pulp stem cells with self-setting biphasic calcium phosphate cement, *J. Biomed. Mater. Res., Part B*, 2020, **108**(4), 1669–1678.
32 S. K. Wong, Y. H. Wong, K. Y. Chin and S. Ima-Nirwana, A Review on the Enhancement of Calcium Phosphate Cement with Biological Materials in Bone Defect Healing, *Polymers*, 2021, (18), 13.
33 C. Bao, W. Chen, M. D. Weir, W. Thein-Han and H. H. Xu, Effects of electrospun submicron fibers in calcium phosphate cement scaffold on mechanical properties and osteogenic differentiation of umbilical cord stem cells, *Acta Biomater.*, 2011, **7**(11), 4037–4044.
34 F. He and J. Ye, *In vitro* degradation, biocompatibility, and *in vivo* osteogenesis of poly(lactic-*co*-glycolic acid)/calcium phosphate cement scaffold with unidirectional lamellar pore structure, *J. Biomed. Mater. Res., Part A*, 2012, **100**(12), 3239–3250.
35 S. Maenz, O. Brinkmann, E. Kunisch, V. Horbert, F. Gunnella and S. Bischoff, *et al.*, Enhanced bone formation in sheep vertebral bodies after minimally invasive treatment with a novel, PLGA fiber-reinforced brushite cement, *Spine J.*, 2017, **17**(5), 709–719.
36 Y. Wang, H. Wu, Z. Wang, J. Zhang, J. Zhu and Y. Ma, *et al.*, Optimized Synthesis of Biodegradable Elastomer PEGylated Poly(glycerol sebacate) and Their Biomedical Application, *Polymers*, 2019, (6), 11.
37 Y. Ma, W. Zhang, Z. Wang, Z. Wang, Q. Xie and H. Niu, *et al.*, PEGylated poly(glycerol sebacate)-modified calcium phosphate scaffolds with desirable mechanical behavior and enhanced osteogenic capacity, *Acta Biomater.*, 2016, **44**, 110–124.
38 X. Li, F. He and J. Ye, Preparation, characterization and *in vitro* cell performance of anti-washout calcium phosphate cement modified by sodium polyacrylate, *RSC Adv.*, 2017, **7**(52), 32842–32849.
39 H. Zhou, Z. He, Y. Cao, L. Chu, B. Liang and K. Yu, *et al.*, An injectable magnesium-loaded hydrogel releases hydrogen to promote osteoporotic bone repair *via* ROS scavenging and immunomodulation, *Theranostics*, 2024, **14**(9), 3739–3759.
40 R. Zhao, S. Chen, W. Zhao, L. Yang, B. Yuan and V. S. Ioan, *et al.*, A bioceramic scaffold composed of strontium-doped three-dimensional hydroxyapatite whiskers for enhanced bone regeneration in osteoporotic defects, *Theranostics*, 2020, **10**(4), 1572–1589.